In Situ Electro-Mechanical Experiments and Mechanics Modeling of Fracture in Indium Tin Oxide-Based Multilayer Electrodes**

By *Cheng Peng, Zheng Jia, Henry Neilson, Teng Li* and Jun Lou**

Indium Tin Oxide (ITO) films are widely used as transparent electrodes in electronic displays and solar cells. However, the small fracture strain of brittle ITO films poses significant challenge to their applications in flexible electronics devices that often undergo large deformation. Inspired by recent development of inorganic/organic hybrid permeation barriers for flexible electronics, we design and fabricate ITO-based multilayer electrodes with enhanced electro-mechanical durability. In situ electro-mechanical experiments of five structural designs of ITO-based multilayer electrodes are performed to investigate the evolution of crack density and the corresponding variance of electrical resistance of such electrodes. A coherent mechanics model is established to determine the driving force for crack propagation in the ITO layer in these electrodes. The mechanics model suggests that a top protective polymeric coating above and an intermediate polymeric layer below the ITO layer can effectively enhance the mechanical durability of the ITO electrodes by reducing the crack driving force up to 10-folds. The modeling results offer mechanistic understanding of the in situ experimental measurements of the critical fracture strains of the five types of ITO-based multilayer electrodes. The findings in this work provide quantitative guidance for the material selection and structural optimization of ITO-based multilayer transparent electrodes of high mechanical durability.

Indium Tin Oxide (ITO) is one of the most widely used transparent conducting oxides in applications such as electronic displays and solar cells. The low resistivity and high transmittance of ITO have led to the recent explorations of polymer-supported ITO films as the transparent electrodes in flexible electronics. Flexible devices are often subject to repeated large deformation. While compliant polymer sub-strates can sustain large strain, brittle ITO films often fracture at a small strain. The cracking of ITO electrodes leads to loss of electrical conductance, posing crucial challenge to the reliability of flexible devices. As an effort to address this challenge, here we report a multilayer structural design of ITO-based electrodes with enhanced electro-mechanical durability. In particular, our in situ electro-mechanical experiments and coherent mechanics modeling reveal that, a top protective polymeric coating above and an intermediate polymeric layer below the ITO electrode can effectively reduce the driving force for cracking of the ITO electrode. The findings of the present paper suggest a feasible solution to durable transparent electrodes for flexible electronics.

The multilayer structural design of ITO-based electrodes in the present study is inspired by the recent progress in designing high performance permeation barriers for flexible electronics. While flexible electronics is being developed toward an array of promising applications (e.g., paper like displays and sensitive electronic skins, etc.),[1–6] the service life of flexible devices is limited due to the vulnerability of functional organic layers in flexible devices to the attack of environmental water vapor and oxygen. High performance

[*] C. Peng, H. Neilson, Prof. J. Lou
Department of Mechanical Engineering and Materials
Science, Rice University, 6100 Main Street MS 321,
Houston, TX 77005, USA
E-mail: jlou@rice.edu
Z. Jia, Prof. T. Li
Department of Mechanical Engineering and
Maryland Nano Center, University of Maryland,
2181 Glenn L. Martin Hall, College Park, MD 20742, USA
E-mail: lit@umd.edu

permeation barriers are desired to achieve long-lasting flexible electronics devices. However, designing such permeation barriers to allow a reasonable service life of flexible devices is rather challenging, given the design criteria over three orders of magnitude more stringent than that of traditional barriers in terms of water vapor permeation rate and the large deformation of the flexible devices.[7,8] Recently, organic-inorganic multilayer permeation barriers (e.g., alternating layers of polyacrylate and Al_2O_3) are emerging as a promising solution to the stringent barrier requirement of flexible electronics.[7,9,10] In such multilayer permeation barriers, the inorganic layer serves as the barrier for water vapor and oxygen and the organic layers decouple the defects (e.g., pinholes) in the as-made inorganic layers and thus yield a remarkably elongated diffusion path for water and oxygen molecules. Modeling study of the failure mechanics of multilayer permeation barriers shows that the organic layers can also increase the critical fracture strain of the inorganic layers.[11,12] A recent study further reveals that a compliant protective coating on the top inorganic layer in a multilayer permeation barrier can further enhance the mechanical durability of the permeation barriers.[12]

Motivated by the progress in the abovementioned multilayer permeation barriers, we design and fabricate ITO-based multilayer electrodes with enhanced electro-mechanical durability. The failure mechanics of the ITO-based multilayer electrodes will be investigated through both in situ electro-mechanical experiments of the electrodes and coherently devised mechanics modeling. So far, existing studies on inorganic/organic multilayer permeation barriers for flexible electronics are mainly based on modeling and no systematic experimental study of their failure mechanics has been reported. In this sense, results from the present paper could also potentially lead to a better understanding of the failure mechanisms of multilayer permeation barriers.

The rest of the paper is organized as follows. Section 1 first describes five structural designs of ITO-base multilayer electrodes and the fabrication procedure, and then reports in situ electro-mechanical tests of these five types of ITO-based multilayer electrodes inside a scanning electron microscopy (SEM) chamber, in which the cracking evolution in the ITO layer and the corresponding variation of electrical resistance of the electrode can be monitored in real time as the function of applied tensile strain. Section 2 delineates a coherent mechanics model to determine the dominating fracture modes of the five types of ITO-based multilayer electrodes and to compute the driving force of crack propagation in the ITO layer of these multilayer electrodes. Results from the mechanics modeling offers a mechanistic understanding of the dependence of critical fracture strains of the ITO-based multilayer electrodes on the structural design as measured through in situ experiments. The main research findings of this paper are summarized in Section 3.

1. Experimental Results

1.1. Design and Fabrication of Five Different Structures of ITO-based Multilayer Electrodes

Five different structures of ITO-based multilayer electrodes are designed and fabricated, and schematics of the cross-section view of these five structures are showed in Figure 1. The polyethylene terephthalate (PET, 127 μm thick) in well-cut dog-bone shape (gauge length and width are 7 and 3 mm, respectively) is employed as the substrate. The PET substrate is first coated by an Al_2O_3 (60 nm thick) layer using e-beam evaporation method (Sharon E-Beam Evaporator). In Structure 1, an ITO layer (80 nm thick) is further coated directly on top of the Al_2O_3 layer, using e-beam evaporation method. In Structure 2, an intermediate polymeric layer of polymethyl methacrylate (PMMA, 495A2 from MicroChem Corp.) is first coated onto the surface of the Al_2O_3 layer by spin coating method with the speed of 1000 rms for 30 s, and the resulting thickness of PMMA is about 100 nm. An ITO layer (80 nm thick) is then coated on top of the PMMA layer. In Structure 3, S1813 (Shipley Microposit S1813 photoresist) is used as intermediate polymeric layer between the Al_2O_3 and ITO layers and is spin coated with the speed of 3000 rms for 30 s with a resulting thickness about 1 μm. In Structures 4 and 5, a layer of PMMA (100 nm thick) and S1813 (1 μm thick) is spin coated on top of the ITO layer of Structure 3, respectively, serving as a top protective coating. The thicknesses of various layers in these five structure designs are determined by an atomic force microscope (Digital Instrument Nanoscope IIIA), using the contact mode. To ensure the well bonding in between layers in all five designs, a 5 nm thick Cr layer (not shown in Figure 1 for visual clarity) is coated between adjacent layers by e-beam evaporation method.

1.2. In Situ SEM Observation of Channel Cracks in ITO Film under Uni-Axial Tension

To characterize the channel cracks initiation and propagation of the ITO layers in different multilayer electrode structures, in situ uni-axial tensile tests are performed inside a SEM chamber. The in situ tensile tests are of particular importance to correlate crack initiation and propagation process with the applied tensile strain, and to avoid the unloading-induced partial or full closure of cracks in the ITO
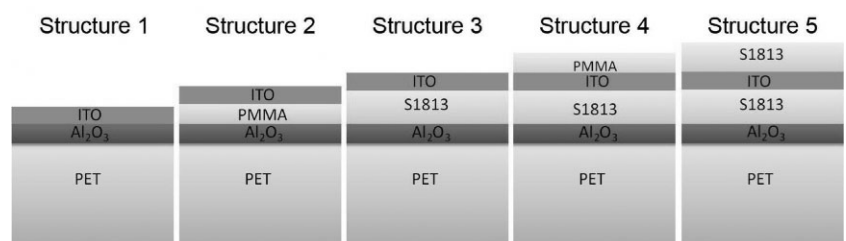
Fig. 1. Schematics of five structural designs of ITO-based multilayer electrodes. The thicknesses of PET, Al_2O_3, ITO, PMMA, and S1813 are 127 μm, 60 nm, 80 nm, 100 nm, and 1 μm, respectively. A 5 nm Cr layer is coated between adjacent layers to increase interlayer adhesion (not shown for visual clarity).
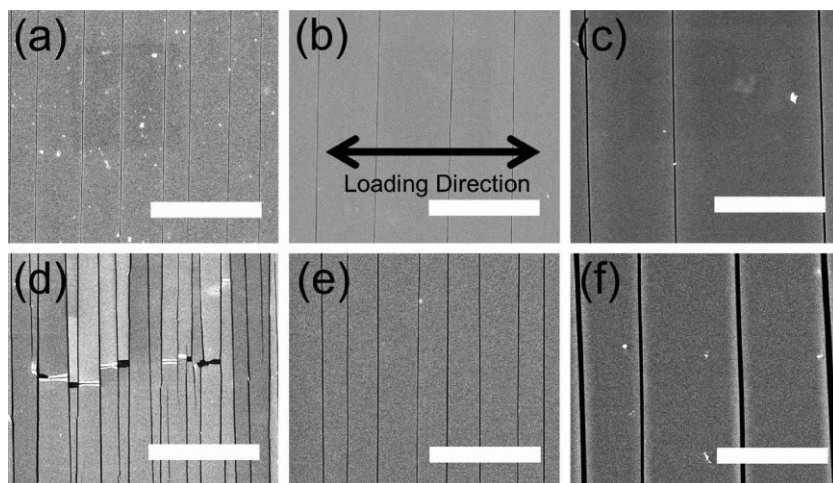
Fig. 2. In situ observation of multilayer structures in different strain levels: (a) Structure 1, (b) Structure 2, and (c) Structure 3 are at the strain of ≈4%; and (d) Structure 1, (e) Structure 2, and (f) Structure 3 are at the strain of ≈13%. The morphology of top ITO layer was recorded by taking SEM images from the top view. The white scale bar in each figure is 30 μm in length, and the arrow indicates the loading direction.

layer in ex situ tests. The detail description of the experimental method can be found in our earlier paper.[13]

The channel crack initiation and propagation process in the ITO layer in Structures 1, 2, and 3 are quite similar: ITO layers are very smooth, without any appreciable cracks before loading; as the tensile strain increases to a threshold value, small channel cracks start to initiate at the edges of sample and then grow along the sample width direction, perpendicular to the tensile loading direction. Figure 2 shows a series of snapshots of these multilayer electrodes during tensile loading. Some interesting phenomena are found as following. First, the channel crack distribution in the ITO film is quite uniform along the sample length direction (also the loading direction), which suggests that the rather uniform elongation of the PET substrate. Second, as the strain level increases, the number of channel cracks in the same structure would increase, e.g., the number is only 4 in Figure 2(b) but 8 in Figure 2(e). Finally, at the same strain level, the number of cracks is affected by the existence and thickness of the intermediate polymer layer: the number of cracks can be reduced after inserting a thin polymer layer in Structure 2,

compared to Structure 1 [Figure 2(a and b), and Figure 2(d and e)], even the thickness of the polymer is on the same order of Al_2O_3 barrier and ITO function layer (100 nm PMMA, 60 nm Al_2O_3, and 80 nm ITO); and the number of cracks can be further reduced if the polymer thickness is increased in Structure 3 (1 μm S1813), compared to Structure 2 [Figure 2(b and c), and Figure 2(e and f)]. It is worth noting that, when Structure 1 is subject to severe tension, some ITO strips (demarcated by two neighboring channel cracks) delaminate and buckle away from the substrate [e.g., Figure 2(d)], driven by the compressive stress in the ITO film due to the Poisson's effect. Severe bending due to buckling results in high tensile stress near the top surface of the buckled crest of the ITO strip, which eventually leads to the ITO cracking at the crest along the direction roughly parallel to the applied tension.[14]

To quantitatively describe the channel cracking under applied tensile strain, we define crack density as the number of channel cracks per unit length in the tensile loading direction. The crack density as a function of the applied tensile strain in Structures 1 to 3 is shown in Figure 3(a). For each structure, the crack density first increases significantly as the applied strain increases, and then gradually saturates at certain value. The sample without any intermediate polymeric layer (Structure 1) has the highest value of saturating crack density, while the sample with the thicker S1813 intermediate polymeric layer has the lowest value of saturating crack density (Structure 3). Both qualitative observation and quantitative results of the evolution of crack density at various applied strains indicate that the intermediate PMMA layer in Structure 2 can effectively reduce the crack density when compared with that in Structure 1, and the crack density can be further reduced when a thicker and stiffer intermediate polymeric layer is used (Structure 3).
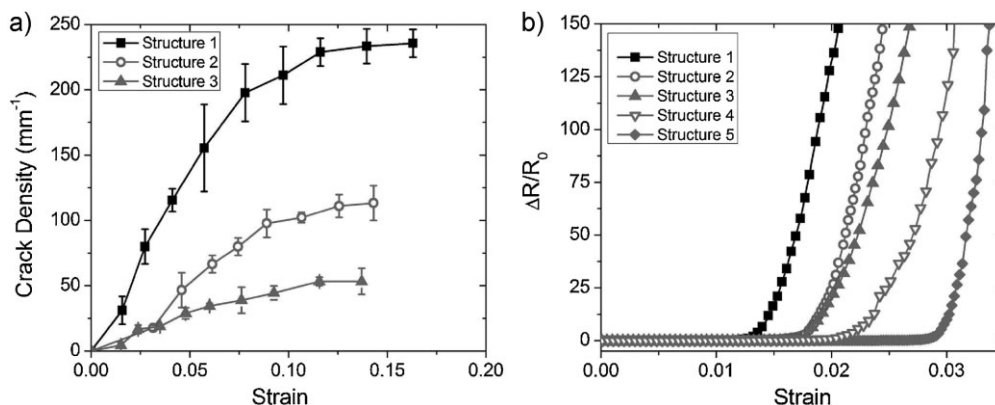
Fig. 3. (a) Cracks density and (b) normalized change in electrical resistance as the function of strain in different ITO-based multilayer electrodes.

Table 1. *Critical strains of ITO-based multilayer electrodes. The value range of critical strain in each structure was determined from at least three electro-mechanical tests.*

Structure number	1	2	3	4	5
Critical strain (%)	1.0–1.3	1.7–1.9	1.7–1.9	2.1–2.3	2.5–2.8

1.3. Electro-Mechanical Behavior of ITO-Based Multilayer Electrodes

In real applications of flexible electronics, the strain level should be less than that for the initiation of channel cracks in functional layers, and that strain level is always less than 3% in ITO-based electrodes.[15] Other than mechanical failure, conductive failure, defined as the dramatic increase in electrical resistance during deformation, is also employed to evaluate the electro-mechanical quality of electrodes in a more direct and effective way. Figure 3(b) plots the normalized change in electrical resistance as a function of the applied tensile strain. For each multilayer electrode, the electrical resistance of the ITO thin film remains nearly unchanged when the applied tensile strain is relatively small. In other words, the ITO thin film remains electrically conductive when subject to a modest elongation. As the applied tensile strain further increases, the electrical resistance first rises gradually, and then shoots up dramatically, leading to the conductive failure. The critical strain of an ITO-based multilayer electrode is defined as the strain when the normalized change in electrical resistance starts to shoot up dramatically, and the value ranges of critical strain for all the electrodes are listed in Table 1. It is found that the value of critical strain in Structure 1 is the smallest. More importantly, the critical strain is affected by the existence of the intermediate layer: the value of critical strain is increased after inserting the intermediate polymeric layer (PMMA or S1813) in Structure 2 or 3. However, not like the crack density, the thickness of the intermediate polymeric layer seems to play little role in the critical strain: there is nearly no difference of critical strains between Structure 2 and 3.

The above results clearly show that the intermediate polymeric layer can reduce the density of channel cracks in high strain level (>4%) and increase the electrical stability in low strain level (<3%). It has been previously shown that the mechanical durability of the top oxide layer in a multilayer structure can be enhanced by applying a thin protective coating onto the surface of the top oxide.[12] In this work, we coat a polymeric layer (thin PMMA or thick S1813) on top of the ITO thin film (Structures 4 and 5), aiming to increase the electro-mechanical properties during the tensile loading. The results in Figure 3(b) clearly show that the critical strain has been increased after the protective coating, and this is a clear evidence for the improvement of electro-mechanical quality in multilayer structures. In particular, the critical strain of Structure 5 is even higher than that of Structure 4, indicating that a thicker polymeric layer offers more mechanical constraint, which leads to a reduced driving force for the channel cracking of ITO layer.

2. Mechanics Modeling and Results

To understand the dependence of the critical strains of ITO electrodes [as in Table 1 and Figure 3(b)] on the multilayer structural design, we next establish a mechanics model to compute the driving force for steady state channel/tunnel cracking of the ITO electrodes in Structures 1 to 5. Results from our mechanics modeling offer a mechanistic understanding of the role of intermediate and top protective polymeric layers on the improvement of electro-mechanical durability of ITO electrodes.

2.1. Dominating Failure Modes of ITO-Based Multilayer Electrodes

It has been shown that,[11] for a multilayer structure such as Structures 2 to 5 under tension, if the intermediate polymeric layer is thicker than the ITO layer, channel cracking of the top ITO layer in Structures 2 and 3 (or tunnel cracking of the ITO layer in Structures 4 and 5) requires the least driving force when compared with other tensile-cracking failure modes, such as tunnel cracking of the intermediate polymeric layer or channel cracking of ITO/polymer/Al$_2$O$_3$ as a whole. In our multilayer design of Structures 2 to 5, both PMMA and S1813 layers are thicker than the ITO layer. Therefore, channel/tunnel cracking of the ITO layers is expected to be the dominating failure mode in Structures 2 to 5, which agrees with our experimental observation.
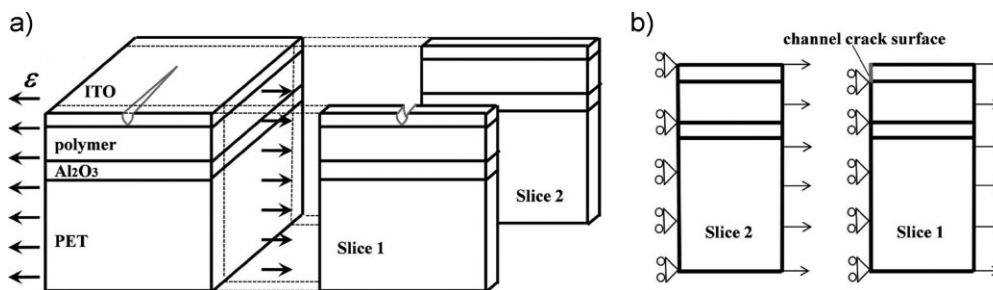
Fig. 4. *(a) The elastic energy reduction associated with the steady state channel cracking propagation in the multilayer can be computed by subtracting the elastic energy stored in a slice of the multilayer structure of unit thickness far behind the crack front (Slice 1) from that far ahead of the crack front (Slice 2). (b) Schematics of models of Slice 1 and Slice 2 used in finite element simulations.*

For Structure 1, however, the ITO layer directly lies on the Al_2O_3 layer without any intermediate polymeric layer in between. Under tension, there may exist two possible failure modes of Structure 1. In failure mode (a), channel cracks occur only in the top ITO layer while the Al_2O_3 layer remains intact, while in failure mode (b), channel cracks cut through the whole thickness of both ITO and Al_2O_3 layers. To determine dominating failure mode of Structure 1, we next compute the critical fracture strains corresponding to the above two failure modes, the lower of which determines the dominating failure mode.

Taking all materials in the multilayer structure to be linearly elastic, the steady state channel cracking propagation is driven by the associated reduction of elastic energy in the multilayer due to crack opening. This elastic energy reduction can be computed by subtracting the elastic energy stored in a slice of the multilayer structure of unit thickness far behind the crack front (Slice 1) from that far ahead of the crack front (Slice 2), as illustrated in Figure 4(a). When the thickness of the intermediate polymeric layer in Figure 4(a) vanishes, it corresponds to Structure 1. Assuming a uniform spacing s between neighboring channel cracks (i.e., $1/s$ is the crack density), dimensional analysis leads to the following form of the elastic energy reduction in Structure 1

$$U = E'_{ITO}\varepsilon^2 h_{ITO}^2 f\left(\frac{h_{ITO}}{h_{Al_2O_3}}, \frac{E_{ITO}}{E_{Al_2O_3}}, \frac{h_{ITO}}{s}\right) \tag{1}$$

where $E'_{ITO} = E_{ITO}/(1 - v_{ITO}^2)$ is the plane strain Young's Modulus of ITO, ε is the applied tensile strain. $h_{ITO}(h_{Al_2O_3})$ and $E_{ITO}(E_{Al_2O_3})$ are the thickness and Young's Modulus of ITO (Al_2O_3), respectively, and v_{ITO} is the Poisson's ratio of ITO. The dimensionless function f denotes the normalized energy released rate of ITO film cracking and can be calculated numerically using finite element method. For clarity, the dimensionless functions f for failure modes (a) and (b) are designated as f_a and f_b, respectively. For failure mode (a), channel cracks will propagate in the ITO layer if the associated reduction of elastic energy U_a exceeds the fracture toughness of ITO, Γ_{ITO}, times the thickness of the ITO layer. Therefore the critical condition can be given as

$$U_a = \Gamma_{ITO}h_{ITO} \tag{2}$$

A combination of Eqs. (1) and (2) gives the normalized critical applied strain ε_a for crack propagation in the ITO layer

$$\frac{\varepsilon_a}{\sqrt{\Gamma_{ITO}/E'_{ITO}h_{ITO}}} = \sqrt{\frac{1}{f_a}} \tag{3}$$

For failure mode (b), cracks channel through the whole thickness of ITO and Al_2O_3 layers, therefore, the associated reduction of elastic energy is

$$U_b = \Gamma_{ITO}h_{ITO} + \Gamma_{Al_2O_3}h_{Al_2O_3}, \tag{4}$$

where $\Gamma_{Al_2O_3}$ is the fracture toughness of Al_2O_3. A combination of Eqs. (1) and (4) gives the critical strain ε_b for channel

cracking propagation in both ITO and Al_2O_3

$$\frac{\varepsilon_b}{\sqrt{(\Gamma_{ITO}h_{ITO} + \Gamma_{Al_2O_3}h_{Al_2O_3})/E'_{ITO}h_{ITO}^2}} = \sqrt{\frac{1}{f_a}} \tag{5}$$

In our specimens, $h_{Al_2O_3} = 0.75h_{ITO}$. For simplicity, the fracture toughnesses of ITO and Al_2O_3 are taken to be identical, i.e., $\Gamma_{ITO} = \Gamma_{Al_2O_3}$. Equation (5) can then be reorganized as

$$\frac{\varepsilon_b}{\sqrt{\Gamma_{ITO}/E'_{ITO}h_{ITO}}} = \sqrt{\frac{1.75}{f_b}} \tag{6}$$

Dimensionless functions f_a and f_b are calculated by normalizing the elastic energy reduction U associated with channel crack propagation. As aforementioned, this elastic energy reduction can be computed by subtracting the elastic energy stored in a slice of the multilayer structure of unit thickness far behind the crack front (Slice 1) from that far ahead of the crack front (Slice 2), as illustrated in Figure 4(a). The elastic energy stored in Slice 1 and Slice 2 can be directly calculated using finite element code ABAQUS. Schematics of models used in finite element calculation for Slices 1 and 2 are given in Figure 4(b). The width s of the model is defined by the inverse of crack density. Taking advantage of symmetry, only half of the slice is modeled and symmetric boundary condition is set for the left edge of the model (in Slice 1, the ITO portion of the left edge is set free to simulate the free channel crack surface); a horizontal displacement $u/2$ is set along the right edge of the model. Therefore, the quantity u/s defines the applied strain. In the finite element calculations, the Young's moduli of ITO, Al_2O_3, and PET are set to be 200, 300, and 2 GPa, respectively, and their Poisson's ratios are 0.3, 0.3, and 0.4, respectively. The thickness of the PET substrate is set to be $625h_{ITO}$. The whole model is meshed with the second-order eight-node quadrilateral elements, with densified mesh in the region near the crack tip. The elastic energy stored in Slice 1 and Slice 2 can be readily calculated.

Table 2 lists the calculated normalized critical strains for failure modes (a) and (b) for three different crack densities. For all crack densities considered, the critical strains for failure mode (b) is always lower than those for failure mode (a). In other words, for Structure 1, the dominating failure mode is the channel cracking through the whole thickness of ITO and Al_2O_3 layers. This can be understood as follows. For failure mode (a), the opening of the channel cracks in the top ITO

Table 2. Normalized critical strains for failure modes (a): channel cracking in the top ITO layer and failure mode (b): channel cracking in both ITO and Al_2O_3 layers for various crack densities.

	Crack density = 10 mm^{-1}	30 mm^{-1}	100 mm^{-1}
$\frac{\varepsilon_a}{\sqrt{\Gamma_{ITO}/E'_{ITO}h_{ITO}}}$	0.518	0.528	0.532
$\frac{\varepsilon_b}{\sqrt{\Gamma_{ITO}/E'_{ITO}h_{ITO}}}$	0.197	0.208	0.226

COMMUNICATION

layer is constrained by the underlying Al$_2$O$_3$ layer. For failure mode (b), the opening of the channel cracks cutting through both ITO and Al$_2$O$_3$ layers is subject to the constraint of the underlying PET substrate. Given the huge difference in the Young's moduli of Al$_2$O$_3$ and PET, the mechanical constraint of the Al$_2$O$_3$ layer in failure mode (a) is much stronger than that of the PET substrate in failure mode (b). Consequently, under tension, Structure 1 is vulnerable to channel cracking through the whole thickness of ITO and Al$_2$O$_3$ layers.

2.2. Comparing Driving Forces for Crack Propagation in Structures 1 to 5

We next compute the driving forces for the steady state channel/tunnel cracking in Structures 1 to 5. The comparison of such driving forces provides mechanistic understanding of the dependence of the measured critical strains of ITO electrodes on the multilayer structural design. The driving forces of cracking for Structures 1 to 5 are defined as

$$G_i = \frac{U_i}{h_i} = \frac{E'_{ITO}\varepsilon^2_{appl}h^2_{ITO}f_i}{h_i} \quad i = 1,\ldots,5 \qquad (7)$$

where U_i is the associated reduction of elastic energy due to crack propagation in Structure i as defined in Eq. (1), h_i is the total thickness of the cracked layers ($h_i = 1.75h_{ITO}$ for Structure 1 and $h_i = h_{ITO}$ for Structures 2 to 5). The values of the dimensionless function f_i are computed using finite element method, with similar strategy delineated in Section 2.1. Here, PMMA and S1813 are modeled as linear elastic materials with Young's modulus of 2 and 7 GPa, respectively, and Poisson's ratio of 0.4 for both.

Figure 5 plots normalized driving force for cracking propagation $G_i/E'_{ITO}\varepsilon^2_{appl}h_{ITO}$ in Structures 1 to 5 as a function of crack density. In the range of crack density we study (i.e., 10–100 mm^{-1}), $G_1 > G_2 > G_3 > G_4 > G_5$. In other words, for a given fracture toughness of the ITO layer, Structure 1 has the lowest critical strain to lose electronic conductance of the
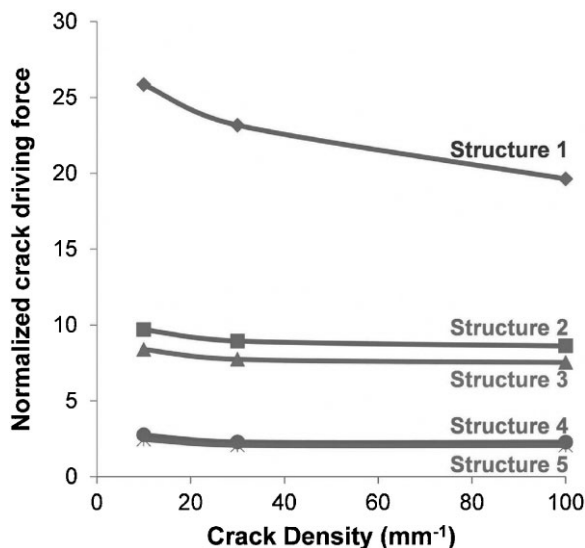
Fig. 5. Normalized driving force for cracking propagation $G_i/E'_{ITO}\varepsilon^2_{appl}h_{ITO}$ in Structures 1 to 5 as a function of crack density.

ITO electrode while Structure 5 has the highest critical strain. Such a prediction of the dependence of critical strain on the structural design agrees with the experimental measurements as shown in Table 1 and Figure 3(b). Such dependence can be further understood as follows. In Structures 2 and 3, the deformable intermediate polymeric layer prevents the channel cracks in the ITO layer from penetrating into the Al$_2$O$_3$ layer. In turn, the intact stiff Al$_2$O$_3$ can offer relatively strong mechanical constraint to the ITO cracking. By contrast, the Al$_2$O$_3$ layer in Structure 1 fractures with the ITO layer. As a result, there is a more than twofold decrease of crack driving force in Structures 2 and 3 from that in Structure 1, for a given crack density. Since the S1813 intermediate layer in Structure 3 is stiffer and thicker than the PMMA intermediate layer in Structure 2, the overall mechanical constraint on the ITO cracking in Structure 3 is slightly stronger than that in Structure 2. Therefore, $G_2 > G_3$. For Structures 4 and 5, the top protective polymeric layer further constrains the cracking opening displacement of the ITO layer (turning channel cracking into tunnel cracking), which results in an about fourfold decrease of the crack driving force from Structures 2 and 3, for a given crack density. When compared with Structure 1, the overall reduction of the crack driving force in Structure 5 is more than 10-fold. In other words, a thin, compliant and well-bonded top protective layer and an intermediate polymeric layer can effectively enhance the electro-mechanical durability of the ITO-based multilayer electrodes. The above results agree with those in a recent study of the mechanical durability of inorganic/organic multilayer permeation barriers for flexible electronics. The slight decrease of the crack driving force as the increase of crack density as shown in Figure 5 can be explained by the partial mitigation of the stress level in the uncracked portions of the ITO layer due to channel/tunnel crack propagation. More crack propagation (i.e., higher crack density) leads to further reduction of the effective stress level in the ITO layer, and thus the slight decrease of the crack driving force. Experimental results in Table 1 show that the critical failure strains of Structure 5 are higher than those of Structure 4, while the modeling results in Figure 5 show that the driving force for cracking in Structures 5 is only slightly lower than that of Structure 4. For Structures 2 and 3, the experimental results on critical failure strains are nearly identical, but the modeling results in Figure 5 predict a 10–20% difference in their driving forces for cracking. These discrepancies between the experimental and modeling results may be attributed to the assumption of well-bonded interfaces in the multilayer electrodes in our models. In reality, interfacial delamination may occur between the ITO layer and the polymeric layers, which leads to an increased driving force for cracking of the ITO layer.[12]

3. Conclusions

In summary, we perform a coherent study integrating in situ electro-mechanical experiments and mechanics modeling

to investigate the failure mechanics of five structural designs of ITO-based multilayer electrodes under tension. While the experimental results show that a top protective polymeric coating above and an intermediate polymeric layer below the ITO layer can effectively enhance the electro-mechanical durability of the ITO-based multilayer electrodes, the mechanics modeling suggests that this enhanced durability is due to the reduction of driving force for ITO cracking up to 10-folds. The findings in this work can provide quantitative guidance for the material selection and structural optimization of organic-inorganic multilayer structures with high mechanical durability.

[1] S. R. Forrest, *Nature* **2004**, *428*, 911.

[2] G. P. Crawford, Flexible Flat Panel Displays, John Wiley & Sons, Chichester, UK **2005**.

[3] S. P. Lacour, J. Jones, S. Wagner, T. Li, Z. G. Suo, *Proc. IEEE* **2005**, *93*, 1459.

[4] W. S. Wong, A. Salleo, in *Flexible Electronics*, Springer, New York, NY, USA **2009**.

[5] J. A. Rogers, T. Someya, Y. G. Huang, *Science* **2010**, *327*, 1603.

[6] D. J. Lipomi, Z. A. Bao, *Energ. Environ. Sci.* **2011**, *4*, 3314.

[7] J. S. Lewis, M. S. Weaver, *IEEE J. Sel. Top. Quantum Electron.* **2004**, *10*, 45.

[8] A. G. Erlat, M. Yan, A. R. Duggal, in *Flexible Electronics*, Springer, New York, NY **2009**, 413.

[9] G. Nisato, M. Kuilder, P. Bouten, P. Moro, L. O. Philips, N. Rutherford, *SID Symp. Digest Tech. Papers* **2003**, *34*, 550.

[10] L. Moro, T. A. Krajewski, N. Rutherford, O. Philips, R. J. Visser, M. Gross, W. D. Bennett, G. Graff, *PIE-The International Society for Optical Engineering, Organic Light-Emitting Materials and Devices VIII, Denver, CO, USA* **2004**.

[11] N. Cordero, J. Yoon, Z. G. Suo, *Appl. Phys. Lett.* **2007**, *90*, 111910.

[12] Z. Jia, M. B. Tucker, T. Li, *Compos. Sci. Technol.* **2011**, *71*, 365.

[13] C. Peng, Z. Jia, D. Bianculli, T. Li, J. Lou, *J. Appl. Phys.* **2011**, *109*, 103530.

[14] Z. Jia, C. Peng, J. Lou, T. Li, *Thin Solid Films* **2012**, *520*, 6576.

[15] D. R. Cairns, D. C. Paine, G. P. Crawford, *Mat. Res. Soc. Symp. Proc.* **2001**, *666*, F3.24.1.